Dust transport in a magnetized radio-frequency discharge under microgravity conditions

V. Land, W. J. Goedheer,* and M. R. Akdim
FOM Institute for Plasma Physics Rijnhuizen, Association Euratom-Fom, Trilateral Euregional Cluster, P.O. Box 1207, 3430 BE Nieuwegein, The Netherlands
(Received 31 May 2005; published 3 October 2005)

Dust is found in plasmas used in industrial applications, such as microelectronics and solar cell manufacturing, in fusion plasmas, where it is usually the result of plasma-wall interactions, and in plasmas in space, such as planetary atmospheres, cometary tails, planetary rings, interstellar molecular clouds, and star and planet formation regions. In plasma applications, magnetic fields are occasionally used, mainly to confine the plasma. In space, however, magnetic fields are very often present and they may strongly influence the behavior of dusty plasma, for instance in the formation of stars and planets. We extended a fully self-consistent two-dimensional fluid model for radio-frequency discharges by adding a homogeneous axial magnetic field and the effect it has on the transport of plasma species in a low-temperature dusty discharge. We show that the magnetic field has an important effect on the (ambipolar) diffusion of ions and electrons in the bulk of the discharge. This causes an important change in the force balance of the dust particles and in the time scales of the formation of a dust-free void. Finally, we compare the parameters of the modeled discharge with the parameters of a planet formation region around a young stellar object (YSO). We conclude that a magnetic field in both low-temperature rf discharges under micro-gravity conditions and dusty plasmas around YSO's has an important effect on the transport of dust and must be important for the formation of planets and stars.

DOI: 10.1103/PhysRevE.72.046403 PACS number(s): 52.25.Xz, 52.27.Lw, 52.65.−y, 97.21.+a

I. INTRODUCTION

Contrary to our everyday experience, almost all matter in the visible universe consists of plasma [1]. In these plasmas, ions and radicals can form small nanometer-sized clusters through chemical reactions. The formation of these "nanoparticles" has been reported both in thin-film solar cell manufacturing and in the microelectronics industry. The nanoparticles seem to have negative as well as positive impacts on the electronic properties of the manufactured devices [2–4]. Recently, different models have been used to study the formation of nanoparticles, while some of these models included the transport of these nanoparticles through the plasma [5,6].

Through a process that is not well understood, the nanoparticles coagulate to form larger particulates, usually in the micrometer range. We will refer to these particulates as "dust particles." The Coulomb interaction for the nanoparticles is not very important since their charge is low, for sizes up to a few nanometers [5]. The coagulation process is therefore believed to involve impact coagulation by Brownian motion or Van der Waals (or dipole-dipole) interactions [7]. The latter force typically goes as $\propto 1/r^6$ and is therefore important only when the nanoparticles come very close to each other.

Once the size of the coagulate reaches the submicron or micron range $\sim 0.1-10\ \mu$m, the plasma-dust and dust-dust interactions become dominant and determine the transport of the dust particles through the plasma. Micron-sized dust particles collect a significant amount of electrons and ions and their charge can be tens of thousands of elementary charges. Due to the high mobility of the electrons (compared to that of the ions), dust particles become mostly negatively charged. The plasma-dust interactions include the *electrostatic force*, i.e., the acceleration of the charged dust particles in the plasma potential, the *neutral drag* caused by friction with the background neutral gas, the *thermophoretic force* which is due to temperature gradients in the background gas and which accelerates the dust particles towards the colder regions, *gravity* and the *ion drag force*, which is caused by the deflection and collection of ions by the charged dust particles, and the corresponding transfer of momentum from the ions to the dust particles. Small dust particles have also been observed to show gyromotion in the presence of a magnetic field and for low background gas pressure [8]. The dust-dust interaction is the mutual *Coulomb interaction* between the charged dust particles.

Recent observations have shown that micrometer-sized dust particles are present in plasmas around young stellar objects (YSO's) [9,10]. Since in this case the dust particles are orbiting a heavy central object (we assume in Kepplerian orbits), we can ignore the force of gravity, which in experiments on Earth usually is the dominant force. Observations of matter outflow and jets in YSO's are connected to magnetic activity and magnetic fields. It is therefore important to look at the effect of a magnetic field on the transport of dust in such plasmas.

In this paper, we present numerical results on the effect of an applied magnetic field on the plasma parameters and on the transport of dust in a typical low-temperature, radio-frequency (rf) plasma experiment such as the one used on the International Space Station to study the transport of dust under microgravity conditions [11,12]. We are therefore not concerned with the actual coagulation process of nanoparticles, but start with the introduction of micrometer-sized particles to the plasma. In Sec. II, we describe the reactor geometry and the model used. In Sec. III, we comment on

*Electronic address: goedheer@rijnh.nl

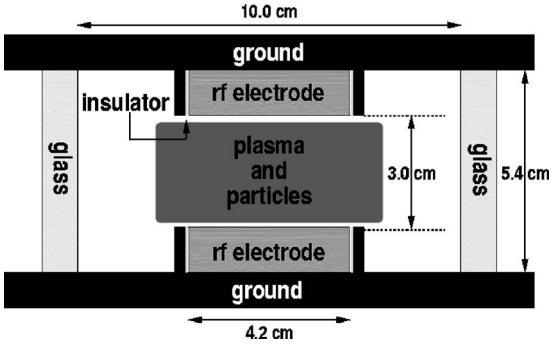

FIG. 1. Sketch of the PKE experiment [11,12] showing the electrodes between which the argon plasma is formed. The dust particles are introduced through both electrodes, with the use of dust injectors or "shakers" placed in the center of the electrodes.

the ion drag force for the typical plasmas that are modeled. Section IV shows the results for different magnitudes of the applied magnetic field. In Sec. V, we will discuss the results and go deeper into the transport of the dust particles. In Sec. VI, we will discuss the role of (ambipolar) diffusion on the transport of plasma particles and on the transport of dust particles induced by the ion drag force. In Sec. VII, we compare the experimental parameters with parameters for a dusty plasma around a young stellar object, and finally in Sec. VIII we will come to conclusions on the effect of the magnetic field on the dust transport and discuss the importance of a magnetic field on the planet formation process.

II. THE EXPERIMENT AND THE MODEL

The geometry we use in our model resembles that of the PKE experiment discussed in [11,12]. Figure 1 shows this geometry. Neutral argon gas is introduced at low pressures between two electrodes powered with a high-frequency (13.56 MHz) potential in push-pull mode and an argon plasma is formed. When the plasma has become stationary, dust particles are introduced through two shakers in the upper and lower electrode. The dust particles are illuminated by a laser sheet and a CCD camera captures the light reflected by the dust particles. The shape of the experiment is a rectangular "box," but we assume that the walls are far away from the plasma and do not influence the plasma properties too much. This way, we can use cylindrical symmetry and restrict ourselves to a two-dimensional (2D) model.

In our model, we use a neutral background pressure of 40 Pa at a peak-to-peak voltage of 100 V. For the simulations presented in this paper, spherical particles with a radius of 6.8 μm are used. Due to the charging of the dust particles, the plasma parameters change with respect to those in a dust-free discharge. Therefore, the plasma and the dust parameters have to be solved self-consistently. We have extended a 2D fluid model for the transport of dust in low-temperature rf plasmas [13] to include the effect of a homogeneous magnetic field on the plasma parameters. We will first describe how the model self-consistently solves the plasma parameters and the dust parameters, then we will discuss the effect of a magnetic field on the transport of plasma species and how this is included in the simulation.

A. The plasma transport equations

The particle balance for the electrons, ions (positive and negative), and metastable atoms is solved using the drift-diffusion approximation. This means that in the particle balance equations for each of the plasma species i,

$$\frac{dn_i}{dt} + \nabla \cdot \mathbf{\Gamma}_i = S_i, \tag{1}$$

the flux is given by a drift term due to the electric field and a diffusive term due to density gradients,

$$\mathbf{\Gamma}_i = n_i \mu_i \mathbf{E} - D_i \nabla n_i, \tag{2}$$

where μ_i is the mobility of species i and D_i is the diffusion coefficient. The electric field $\mathbf{E}$ is found from the Poisson equation including the dust particle charge,

$$\nabla^2 V = -\frac{e}{\epsilon_0}(n_+ - n_e - n_- - Z_D n_D),$$

$$\mathbf{E} = -\nabla V. \tag{3}$$

Z_D is the dust particle charge number, and n_+, n_e, n_-, and n_D are the positive ion, electron, negative ion, and dust particle densities, respectively. The momentum transfer frequency for the argon ions is only several MHz, due to the high ion mass (compared to a GHz for the electrons) and is less than the applied rf. This means that the ions are unable to react to the instantaneous electric field. Instead they "see" an effective electric field $\mathbf{E}_{\text{eff}}$, which is obtained by solving [13]

$$\frac{d\mathbf{E}_{\text{eff}}}{dt} = (\mathbf{E} - \mathbf{E}_{\text{eff}})\nu_{m,+}. \tag{4}$$

By using the effective electric field in Eq. (2), we include inertia effects for the ions in their response to the applied electric field. Note that we solve the ion and electron transport separately and do not assume ambipolar diffusion. The time-averaged fluxes in the shielded center of the discharge, however, are "ambipolar" in the sense that there is no net charge and no net current and that the fastest moving species determines the particle fluxes. So throughout the discussion in the rest of this paper, "ambipolar" diffusion implies the diffusion in the quasineutral part of the plasma, resulting from the coupled transport equations.

The energy balance is solved using a similar drift-diffusion approximation for the average electron energy density $w = n_e \epsilon$, with ϵ the average energy per electron,

$$\frac{dw}{dt} + \nabla \cdot \mathbf{\Gamma}_w = -e\mathbf{\Gamma}_e \cdot \mathbf{E} + S_w. \tag{5}$$

The first term on the right-hand side is Ohmic heating of electrons in the applied electric field, with the electron flux found from Eq. (2), and the source term consists of electron impact collisions, including ionization, recombination on the surface of dust particles, and excitation. These terms are calculated using a two-term Boltzmann solver for the electron energy distribution function. The average electron energy density flux $\mathbf{\Gamma}_w$ is given by

$$\mathbf{\Gamma}_w = \frac{5}{3}\mu_e w\mathbf{E} - \frac{5}{3}D_e \nabla w. \tag{6}$$

For the ions we assume that the energy gained in the electric field is locally dissipated in collisions with the background gas [14]. Together with the heat originating from the surface of the dust particles (see the next subsection), this provides the heating of the background gas.

B. Charging and transport of the dust

Dust particles introduced in a plasma collect ions and electrons and charge up to the floating potential. Once this potential is reached, the currents of electrons and ions toward the surface of the dust particles are equal. For a spherical dust particle, these currents are taken from the orbital motion limited theory (OML) [15]. For a negatively charged particle, they are given by

$$I_+ = 4\pi a^2 e n_+ \sqrt{\frac{E_+}{2m_+}}\left(1 - \frac{eV(a)}{E_+}\right), \tag{7}$$

$$I_e = 4\pi a^2 e n_e \sqrt{\frac{kT_e}{2\pi m_e}} \exp\left(\frac{eV(a)}{kT_e}\right), \tag{8}$$

where E_+ is the energy of the ions consisting of the thermal energy (assuming a Maxwellian distribution) and the kinetic energy from the drift velocity u_+, calculated using Eq. (2),

$$E_+ = \frac{4kT_{\text{gas}}}{\pi} + \frac{1}{2}m_+ u_+^2. \tag{9}$$

In the above equations, a is the dust particle radius, which should be much smaller than the (linearized) Debye length; $a \ll \lambda_D, \lambda_D = (\sqrt{1/\lambda_e^2 + 1/\lambda_i^2})^{-1}$. T_e is the electron temperature and T_{gas} is the gas temperature. Equating $I_+ = I_e$, the equilibrium floating potential $V(a)$ is solved using a Newton iteration method. The dust charge is then given by

$$eZ_d = 4\pi\epsilon_0 a V(a). \tag{10}$$

The densities in the expressions for the current densities are the time-averaged values. Occasionally, very close to the wall, the ion density is much higher than the electron density and the dust charge becomes positive. This results in a loss of dust from these regions.

Once the equilibrium charge is reached, the electrons and ions arriving at the dust particle will recombine at a rate $n_D I_e/e$. The energy released is used to heat up the particle surface, and is radiated away. The dust surface temperature at equilibrium is higher than the gas temperature and the gas colliding with the dust will be heated [13]. This is a heat source for the gas. The temperature profile of the gas, T_{gas}, is obtained by solving the heat conduction equation with heat input from the ions and from the dust.

When the charge on the dust particles is determined, the different forces acting on the dust particles can be calculated. The electrostatic force is simply calculated as

$$\mathbf{F}_{\text{el}} = Z_D e \mathbf{E}_{\text{eff}}. \tag{11}$$

Since we do not include advection of the background gas, the neutral drag acting on the dust particles moving through the gas will simply be

$$\mathbf{F}_n = -\frac{4}{3}\sigma_D \rho_{\text{gas}} v_{\text{th}} \mathbf{v}_D, \tag{12}$$

where $\sigma_D = \pi a^2$ is the geometrical surface of the dust particle, ρ_{gas} is the background gas mass density, v_{th} is the average thermal velocity of the background gas, and $\mathbf{v}_D$ is the drift velocity of the dust particle. The temperature gradients in the background gas cause thermophoretic forces, pushing the particles to cold areas (this is the principle of the "cold trap"). It is calculated using

$$\mathbf{F}_{\text{th}} = -\frac{32}{15}\frac{\sigma_D}{\pi v_{\text{th}}}\kappa_T \nabla T_{\text{gas}}, \tag{13}$$

where κ_T is the translation part of the thermal conductivity. Ions deflected and collected by the charged dust particles transfer momentum to the dust particle, which experience the so called ion drag force. In view of its importance, this force and the assumptions made to calculate it will be discussed separately in Sec. III. It depends on the charge of the dust particle, the Debye length, and the ion flow.

Assuming that the damping neutral drag force balances all the other forces, we can derive a drift-diffusion expression for the dust particle balance, with the dust flux as

$$\mathbf{\Gamma}_D = -\mu_D n_D \mathbf{E}_{\text{eff}} - D_D \nabla n_D - \frac{32}{15}\frac{n_D \sigma_D}{m_D \nu_{m,D} \pi v_{\text{th}}}\kappa_T \nabla T_{\text{gas}} + \frac{n_D \mathbf{F}_{\text{ion drag}}}{m_D \nu_{m,D}}. \tag{14}$$

$\mu_D = eZ_D/m_D\nu_{m,D}$ and the dust diffusion coefficient is taken from [16]. It includes the effect of the mutual Coulomb interaction and the possibility of the formation of crystalline incompressible dust structures,

$$D_D = \frac{1}{\nu_{m,D}}\frac{dP_{\text{cr}}}{dn_D}, \tag{15}$$

$$P_{\text{cr}} = \frac{1 + \beta\kappa}{3\beta} N_{nn} \Gamma P_D \exp(-\beta\kappa). \tag{16}$$

Here, Γ is the ratio of the Coulomb energy over the thermal energy, $\Gamma = (eZ_D)^2/4\pi\epsilon_0 \Delta k T_D$, $\Delta = n_D^{-1/3}$ is the mean distance between dust particles, $\kappa = \Delta/\lambda_D$, and N_{nn} and β are constants depending on the lattice structure of the crystalline dust [17].

The above set of equations is a closed set which allows us to self-consistently solve the plasma parameters and the dust parameters together. For the solution we regularly recalculate the average plasma profiles, in agreement with the actual dust density and charge profiles.

C. Magnetic field

An important extension to the model is the application of a homogeneous axial magnetic field. Charged particles gy-

rate around magnetic field lines, which reduces their mobility and diffusion coefficient perpendicular to the field. The measure of how strong the charged particles are hindered to cross magnetic field lines is given by the "Hall parameter," $\beta_j = \omega_j / \nu_{m,j} (= \mu_j B)$ [18], where $\omega_j = q_j B / m_j$ is the cyclotron frequency and ν_j is the momentum transfer frequency. The diffusion across magnetic field lines is strongly reduced (we call the particles "magnetized") when $\beta \gg 1$. At a neutral pressure of 40 Pa and at room temperature, the ion momentum transfer frequency is about 3 MHz. The electron momentum transfer frequency is approximately 1 GHz. In our simulations, we add a magnetic field $B \leqslant 0.5$ T, so that $\omega_e \leqslant 9$ GHz and $\omega_i \leqslant 0.3$ MHz. We see that the electrons are magnetized, whereas the ions are not. Therefore, we rewrite the mobility and diffusion coefficient for the electrons perpendicular to the magnetic field (thus in the radial direction) as

$$\mu_{e,\perp}(D_{e,\perp}) \rightarrow \left[1 + \frac{e^2 B^2}{m_e^2 \nu_{m,e}^2} \right]^{-1} \times \mu_{e,\perp}(D_{e,\perp}). \quad (17)$$

Even though the ion diffusion coefficient and mobility are not affected by the magnetic field, the ion flux also changes. In the center of the discharge, quasineutrality and the particle balances result in "ambipolar" conditions that couple the ion flux to the electron flux via the average electric field that is generated. Note that the "ambipolar" conditions include the effect of recombination on the dust particles and that in the vicinity of the walls and at the edge of a dust cloud charge separation will occur.

III. THE ION DRAG FORCE

When an ion approaches a charged dust particle, it can be either collected or deflected (scattered) or move along undisturbed when the distance between the ion and the dust particle is large enough. The momentum transferred from the collected and deflected ions causes an acceleration of the dust particle, called the ion drag force. The general expression for the ion drag force is [19]

$$\mathbf{F}_{\text{ion}} = m_+ \int \mathbf{v} v f_+(\mathbf{v}) [\sigma_c(v) + \sigma_s(v)] d\mathbf{v}, \quad (18)$$

where $f_+(\mathbf{v})$ is the ion velocity distribution function, $\sigma_c(v)$ is the (velocity-dependent) collection cross section, and $\sigma_s(v)$ is the scattering cross section. The original approaches to solve the above equation analytically [19,20] assumed that the dust particle is at rest and $a \ll \lambda_D \ll l_+, \Delta \gg \lambda_D$, where l_+ is the ion mean free path.

The collection term is solved from OML theory, which gives the maximum collection cross section as

$$\sigma_c(v) = \sigma_D (1 + 2\rho_0 / a), \quad (19)$$

where $\rho_0 = Z_D e^2 / 2\pi\epsilon_0 m_+ v^2$ is the "Coulomb radius." This way, the collection cross section does not depend on the specific form of the potential around the dust particle. In order to determine the scattering cross section, one should know the exact form of the potential around the dust particle. The approach by Barnes *et al.* [20] assumes that only ions approaching the dust particle very closely are deflected. This means that these ions are assumed to move only through the unscreened Coulomb potential. The scattering cross section can then be found as

$$\sigma_s(v) = 4\pi \int_{\rho_{\min}}^{\rho_{\max}} \frac{\rho d\rho}{1 + (\rho/\rho_0)^2} = 4\pi \rho_0^2 \Lambda, \quad (20)$$

with Λ the Coulomb integral,

$$\Lambda(v) = \frac{1}{2} \ln \left[\frac{\rho_0^2(v) + \rho_{\max}^2(v)}{\rho_0^2(v) + \rho_{\min}^2(v)} \right]. \quad (21)$$

The minimum radius of approach is given by the collection radius $\rho_{\min} = \rho_c$. The maximum radius, or cutoff radius, is then chosen to be the linearized Debye length, $\rho_{\max} = \lambda_D$. It was soon noticed [20,21] that by using the linearized Debye length as the cutoff radius, the calculated ion drag force was about an order of magnitude too low to explain experimental results. Therefore, the electron Debye length was used as the cutoff length instead of the linearized Debye length, which increases the ion drag force with a factor of 5–10. However, this choice of the electron Debye length is only a qualitative improvement; there is no physical basis for this choice. Once the ions are accelerated in the electrode sheath or in an internal sheath adjacent to a dense dust cloud, the ions obtain an energy comparable to the thermal electron energy and the linearized Debye length approaches the electron Debye length. Problems exist mainly in the quasineutral central region, where the ion energy is low.

In [19] it was mentioned that the above approach is only valid when $\alpha = \rho_0 / \lambda_D \ll 1$. They proposed to include scattering by ions with $\alpha > 1$, so called "large angle scattering." Using this approach, the cutoff radius is chosen as $\rho_{\max} = \lambda_D (1 + 2\alpha)^{1/2}$, leading to the revised Coulomb logarithm,

$$\Lambda = \ln \left[\frac{\rho_0(v) + \lambda_D}{\rho_0(v) + a} \right]. \quad (22)$$

Solving Eq. (18) with Eqs. (20) and (21) (Barnes *et al.*) or Eq. (22) (Khrapak *et al.*) gives the ion drag force. Even though there is more physics behind the approach by Khrapak *et al.*, the qualitative result is very similar, which has led to many discussions [22–24]. A recent paper about the formation of a void around a probe performed in the PKE geometry during parabolic flight again shows that the approach of [20] with the electron Debye length gives similar results to the approach of [19], which both agree well with the experimental observations [25].

In these experiments, the neutral density was such that the ratio of the Debye length and the ion mean free path $\lambda_D / l_+ \approx 390\ \mu\text{m} / (\sqrt{2} \times 170\ \mu\text{m}) \approx 1$, in which case collisions do not yet play an important role in the calculation of the scattering ion drag force. Once the ion mean free path becomes less than the Debye length, ion-neutral collisions may influence the ion drag force significantly. In [26,27], Ivlev *et al.* derived the appropriate forms of the ion drag force in the case of subthermal ion flow (as was the case with the above derivations) and suprathermal ion flow, where the thermal Mach number is defined as $M_T = u_+ / v_T$, $v_T = \sqrt{8kT_+ / \pi m_i}$, and

u_+ is found from Eq. (2). For subthermal ion flow and low α, the ion drag force due to scattering is given as

$$\mathbf{F}_{\text{ion}} = \frac{2\sqrt{2\pi}}{3} n_+ m_+ v_T u_+ \rho_0(v_T) \left[\Lambda + \mathcal{K}\left(\frac{\lambda_D}{l_+} \right) \right], \qquad (23)$$

where

$$\mathcal{K}(x) = x \arctan(x) + \left(\sqrt{\frac{\pi}{2}} - 1 \right) \frac{x^2}{1+x^2} - \sqrt{\frac{\pi}{2}} \ln(1+x^2). \qquad (24)$$

In order to assess the importance of the modifications of the ion drag force, we have calculated the values of α, M_T, and the ratio of λ_D/l_+ for the profiles obtained in our simulation. In the bulk of the discharge α becomes very large, due to the fact that the ion flow speed is small, while the computed dust charge is very high. Nevertheless, in [22,24,25] it was shown that the results for the approach by Barnes *et al.* and the approach by Khrapak *et al.* both seem to be in good agreement with experiment. Outside the plasma bulk, α drops to zero rapidly, due to the increase in the ion flow speed (u_+) and a decrease in the computed dust charge resulting from the high value of the ratio n_+T_e/n_eT_+, which means that applying the approach of Khrapak *et al.* there would give similar results to the approach of Barnes *et al.* with the electron Debye length.

For our discharge settings and particle diameter, the ratio of λ_D/l_+ has to exceed a value of 3 in order for the collisions to be important in the calculation of the ion drag force. In the regions of the discharge where this condition is fulfilled, i.e., toward the outer walls of the experiment, where the ion flow speed due to the electric field becomes important, α is much less than unity, which means that the force given by Eq. (23) stays close to the ion drag force calculated with Eq. (22), which, as discussed above, for small α gives similar results to the approach by Barnes *et al.* using the electron Debye length. We have computed that the error we introduce in our simulations by using the approach of Barnes *et al.* with the electron Debye length instead of the approach by Ivlev *et al.* stays within 25%. This error is even less for a higher magnetic field, because in that case the dust charge is lower. We find this percentage acceptable.

The critical Mach number at which the collection force dominates over the scattering force is given by $M_{\text{cr}} = [\rho_0(v_T)/a]^{2/3}$. This can be as low as 6 for the low dust particle charge computed (see Sec. IV) on the outside of the discharge. This is in contrast to what is mentioned in [27] and implies that the collection force becomes more important than the effect of collisions for the larger part of the discharge outside the bulk region. This force is calculated by using the OML theory and is therefore independent of the approach used to calculate the scattering ion drag force. Therefore, we do not consider the solution by Ivlev *et al.* for very high Mach numbers.

In view of the discussions in [22,24,25] and the above conclusions about the importance of collisions in the simulations presented here, we conclude that using the approach by Barnes *et al.* [20] together with the electron Debye length as the cutoff radius, which has proven itself computationally robust and useful [13,28], is still an acceptable approach. As a final note we mention that here we do not consider nonlinear effects due to ion trapping, which leads to a change in the potential around a dust particle [29,30]. Also recent considerations of changes in the potential due to collective behavior of large numbers of dust particles [31] are not considered in this paper. We now continue to discuss the results found from the simulations.

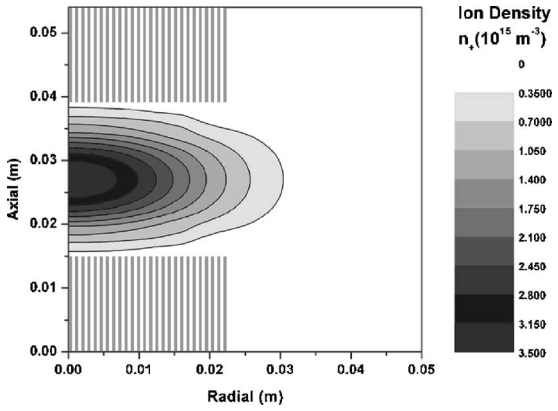

FIG. 2. Time-averaged ion density for a magnetic-field-free dusty discharge. The plasma is mostly formed between the electrodes. We can clearly see the bulk of the discharge as the central maximum in the ion density. No dust particles have been added yet.

IV. DUSTY DISCHARGES WITHOUT MAGNETIC FIELD AND WITH A MAGNETIC FIELD OF $B=0.25$ T

In this section we compare the profiles for a magnetic-field-free dusty discharge and a dusty discharge with a magnetic field of $B=0.25$ T. We use a background pressure of 40 Pa with a 100 V peak-to-peak potential at 13.56 MHz. Please note that we did not consider negative ions (irrelevant for argon) nor metastables in these calculations. We first compare the potential and the ion density. In both discharges the plasma is mainly created between the electrodes, which are the gray-white striped rectangles in the figures.

Figures 2 and 3 show the ion density profiles of the stationary plasma discharges before any dust is introduced. In Fig. 2, no magnetic field is applied. In Fig. 3, the magnetic field applied in the model has a value of $B=0.25$ T. We can see how the ion density profile changes due to *the presence of the magnetic field only*. The quasineutral bulk is extended radially. However, the maximum value of the ion density in the case of an applied magnetic field is less, indicating that the total amount of ions in the discharge is approximately the same. From now on, we compare profiles for dust-free plasmas with profiles at the end of the simulation at which 10^6 dust particles have been added. We can see how the change in the ion density profile induced by the magnetic field changes the plasma and dust parameters.

In Fig. 4, we present the potential profile averaged over one rf cycle, for the magnetic-field-free discharge. We see the quasineutral bulk of the plasma between the electrodes as the equipotential area. In front of the electrodes the large electric fields of the sheath regions appear. Near the end of

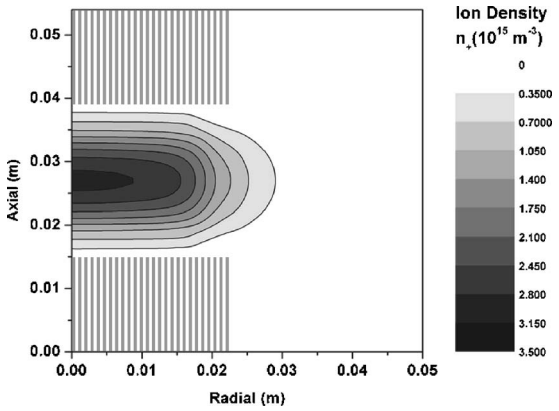

FIG. 3. Time-averaged ion density for the magnetized dusty discharge. The bulk has a cigar-shaped maximum in the ion density, corresponding to the bulk of the plasma, modified by the application of a magnetic field. The maximum value of the ion density is less, indicating that the total number of ions is roughly the same in both discharges. No dust particles have been added.

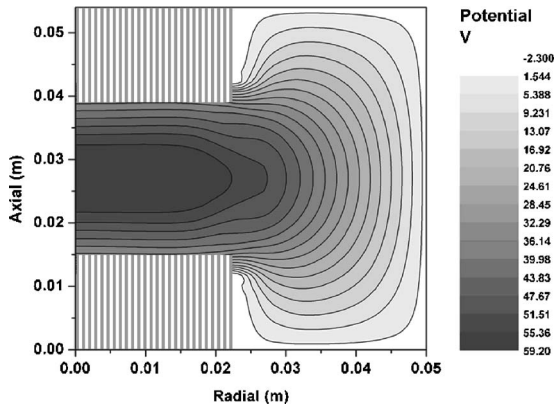

FIG. 5. The time-averaged potential profile for the magnetized dusty discharge. The equipotential of the quasineutral bulk has a cigarlike shape following the ion density profile. In front of the electrodes are the sheath regions, and outside of the electrodes we see the radial and axial electric fields caused by the low mobility of the ions.

the electrodes, the radial electric field changes from approximately zero to an electric field pointing toward the outer walls. This electric field, generated due to the high mobility of the electrons, accelerates the ions toward the outer wall. Figure 5 shows the potential for the magnetized discharge. The potential profile is almost the same, however we see a big change in the electric-field-free bulk of the plasma, which has become cigar-shaped, as the ion density profile. This change in the bulk potential results from the reduced electron mobility in the applied magnetic field. Since the transport is "ambipolar," the ion transport is also affected.

Figures 6 and 7 show the ion density profiles at the end of the simulations, when the dust has reached its equilibrium density profile. Even though the ion density profiles have extended "wings," which are due to the attraction of the ions by the negatively charged dust particles, the bulk of the discharge shows the same ion density profiles as shown in Figs. 2 and 3, with the exception that the recombination of ions (and electrons) on the dust particles has reduced the ion (and electron) density, as was also described in [13]. Clearly, the effect of the magnetic field on the plasma parameters is also important when a large number of dust particles is introduced to the plasma.

The change in ion density is reflected in the dust density profiles. The ions are accelerated out of the center of the discharge, causing the ion drag force which pushes the dust particles out of the center of the discharge. A dust-free void is formed in the center of the discharge. The dust density for the magnetic-field-free discharge, presented in Fig. 8, clearly shows the dust-free void, as well as the dust-free sheath regions. In this case, a local maximum in the dust density is created outside the electrodes, due to the transport of dust particles in the radial direction. For this discharge the time needed to form a closed boundary around the void is 1.15 s (see Sec. V).

Figure 9 shows the dust density for the magnetized case. The void has a very different shape, due to the change in the

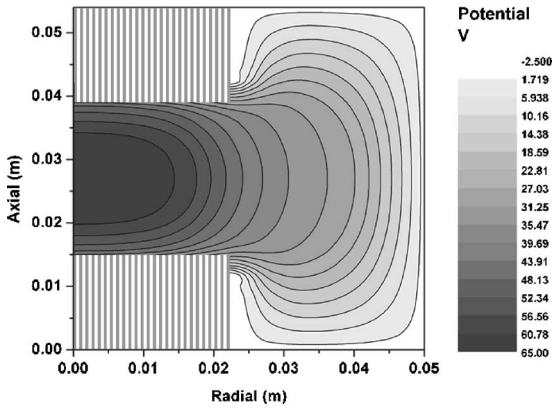

FIG. 4. The time-averaged potential profile for the magnetic-field-free discharge. The equipotential in the center corresponds to the quasineutral bulk of the plasma, where the plasma densities have their maximum. In front of the electrodes, we see the large sheath electric fields. Towards the outer wall we see the electric field causing large drift of ions.

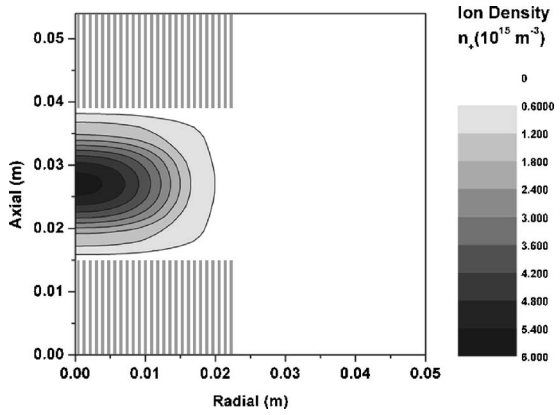

FIG. 6. Time-averaged ion density for a magnetic-field-free dusty discharge. The plasma is mostly formed between the electrodes. The extended wings are the result of attraction by the dust particles. The central maximum corresponds to the electric-field-free bulk in Fig. 4. One can also see the effect of recombination of the ions on dust particles.

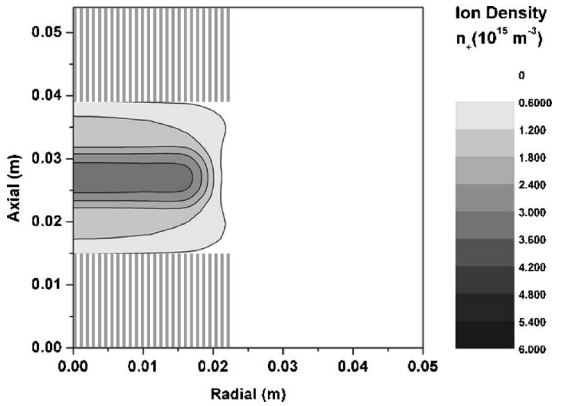

FIG. 7. Time-averaged ion density for the magnetized dusty discharge. The bulk has a cigar-shaped maximum in the ion density, corresponding to the bulk seen in the potential of Fig. 5. The maximum value of the ion density is less, indicating that the total number of ions is roughly the same in both discharges.

ion density profile. The much sharper boundary of the ion density profile causes a much sharper boundary of the dust-free void. We also see that the sheath regions are less clear. The dust charge is slightly less in front of the electrodes in this case (36.000e to 48.000e instead of 43.000e to 49.000e in the unmagnetized case), which means that the electrostatic repulsion is slightly less, moving the force balance between the axial ion drag force and the electrostatic force closer to the electrode surfaces. The most important observation is that for a magnetic-field strength of $B=0.25$ T, a closed boundary around the void is formed *already after* 0.55 s. This means there is a big difference in the dust-transport properties of both discharges. We also observe that there is no distinct maximum in the dust density formed outside of the electrodes.

The dust inserted in the discharge becomes negatively charged, because of the high electron mobility compared to the ion mobility. Due to the high value of n_i/n_e, the increase in ion temperature, and the decrease in electron temperature near the outer wall, the dust charge is low there. This effect

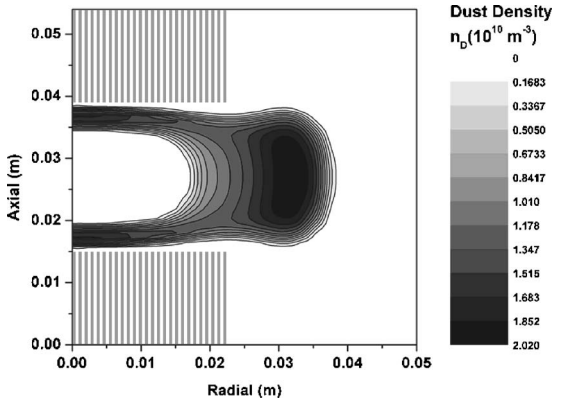

FIG. 8. Dust density profile for a magnetic-field-free dusty discharge. We can clearly see the dust-free void in the center of the discharge. The sheath regions are also dust-free. In this case, we find a local maximum in the density just outside of the electrodes. The closed boundary around the void was formed after ±1.15 s.

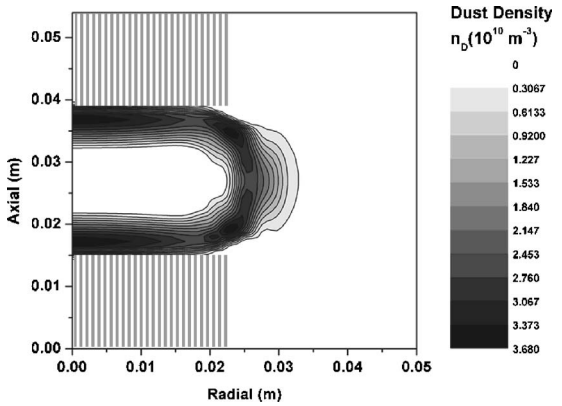

FIG. 9. Dust density profile for a magnetized dusty discharge. The central dust-free void is now clearly cigar-shaped, due to the change in the ion density profile. There is no local maximum in the dust density outside of the electrodes. In this magnetized case, the void was closed after 0.55 s, about twice as fast as in the unmagnetized case.

is even enhanced by the magnetic field. The low dust charge and the increase in the ion flow is also the reason for the decrease in α, as mentioned in Sec. III. The typical amount of electrons on a dust particle in the plasma bulk is 40000 and is plotted in Fig. 10 for the magnetic-field-free discharge. Figure 11 shows how the dust charge in the bulk of the magnetized discharge is almost the same as the dust charge in the unmagnetized discharge. The dust charge near the outer walls is less, however, due to the change in the plasma parameters induced by the magnetic field. Note that the charge per particle is computed everywhere, also in regions without any dust present.

V. DUST TRANSPORT WITH AN APPLIED MAGNETIC FIELD

The most important observation regarding the dust transport is the large reduction in the time needed to form a closed dust-free void. In order to compare the results for different magnetic-field strengths, we define the time when the dust

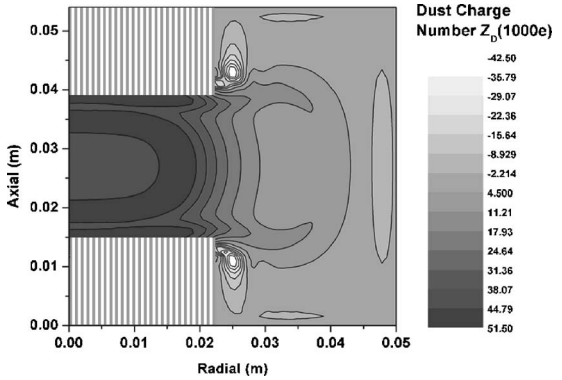

FIG. 10. Number of electrons on a dust particle for a magnetic-field-free dusty discharge. The dust is mainly negatively charged, which results from the high electron mobility compared to the ion mobility. Typical dust charges are 10^4-10^5 electrons.

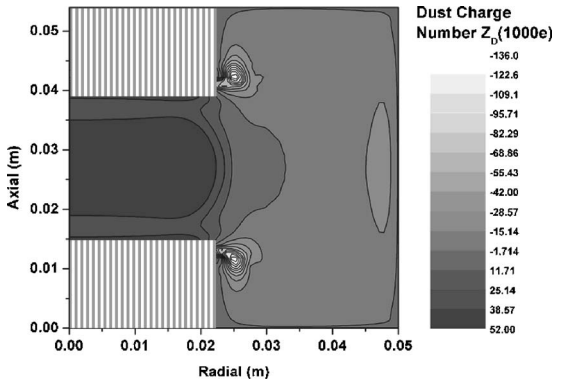

FIG. 11. Number of electrons on a dust particle for the magnetized discharge. The dust charge is again negative. The typical dust charge is similar to that of the unmagnetized discharge, in the order of 10^4–10^5 electrons per dust particle.

sources are turned on as $t=0$. Furthermore, we define the time when a dust-free void is formed as that moment when dust contours of $n_d=8\times10^9$ m^{-3} are closed around the void. This value has no physical meaning, but is chosen only because this value was easy to identify. It would be physically more appropriate to use the coupling parameter as a constraint, for instance by identifying the void formation time as the moment where $\Gamma>\Gamma_{cr}\approx160$ [32], but the coupling parameter becomes very large for small values of the density, which makes it very hard to identify the right time from this criterion. The void formation times found in the simulations are shown in Fig. 12. The error bar indicates the possible error we made in taking the right frame. For higher magnetic fields, the void closes faster and it is more difficult to identify the moment when the dust contours are closed. For low magnetic fields, we estimated that we can be one frame off. For high magnetic fields, we estimate two frames. One frame corresponds to 0.02 s.

We see that for increasing magnetic field, the time needed to form a closed void is decreased by more than a factor of 2.

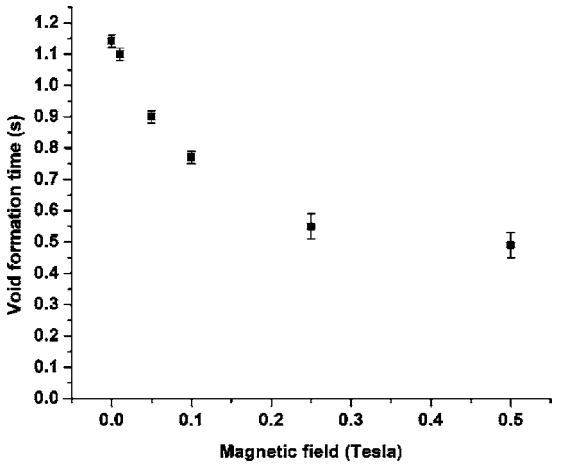

FIG. 12. The time needed to form a closed void. The definition is taken to be closed contours of dust density $n_d=8\times10^9$ m^{-3} around the void. For higher magnetic fields, the time needed to form a closed void becomes much shorter. This means that there is increased transport of dust in the plasma.

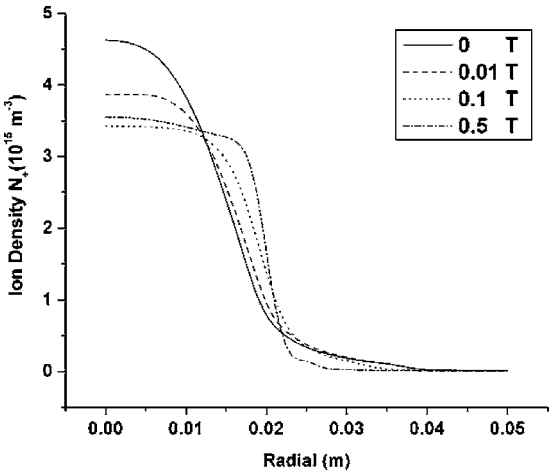

FIG. 13. Time-averaged ion density profiles in plane of symmetry at $z=0.027$ m for different values of the magnetic field. A large quasineutral bulk builds up between the electrodes, together with an increasing gradient at the edge of the electrodes. The increasing gradient is shown in Fig. 14 and plays an important role in dust transport.

This means that either the transport of dust particles through the plasma is increased, or the distance to the force balance point is reduced, or a combination of both factors. In order to understand this reduction in the void formation time, as well as the change in the void shape, we will compare the plasma and dust parameters *at the moment the void is closed*. Since these times are different for different magnetic fields, this also means that the total number of dust particles at these times will be different.

The formation of a dust-free void is the result of dust transport through the plasma. Dust particles will move to points where all the forces acting on them cancel. The two most important forces acting on the dust particles are the ion drag force and the electrostatic force. The thermophoretic force does not play an important role. The electrostatic force pushes the negatively charged dust particles inward, while the ion-drag force is pushing the dust particles toward the outside [33].

The change in the ion density distribution is therefore important for the transport of dust. Figure 13 shows the ion density profiles in the plane of symmetry at $z=0.027$ m. For higher magnetic fields, large gradients appear near the edge of the electrodes at $r=0.021$ m. The quasineutral bulk between the electrodes becomes larger for higher magnetic fields. The total number of ions, which corresponds to the surface under the graphs, remains about equal, which indicates that the total ionization does not change.

Figure 14 shows the gradients in the ion density near the electrode edge. We see that for high magnetic fields, the gradient becomes almost two times the gradient without magnetic field. The change in the gradient has two implications. First, the balance between the electrostatic and the ion-drag force changes. Second, the forces close to the point where all force balances become different. Figure 15 shows the net radial force in the plane of symmetry. The dust particles move to the points where the net force is zero. These points are indicated with the small lines on the horizontal

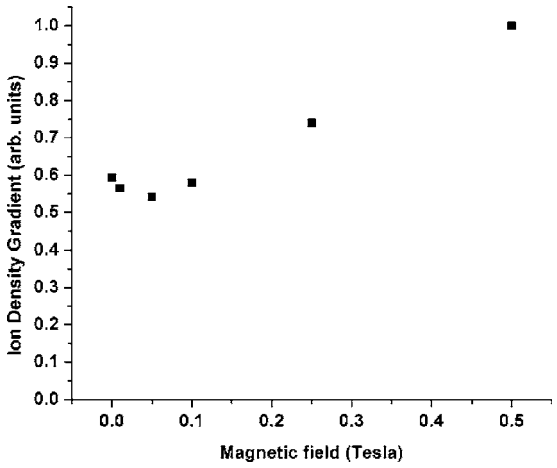

FIG. 14. The radial gradient in the ion density near the edge of the electrode, in the plane of symmetry in arbitrary units. We see how for low magnetic fields the gradient is slightly decreased. For high magnetic fields the gradient becomes larger, which has an important impact on the force balance shown in Fig. 15.

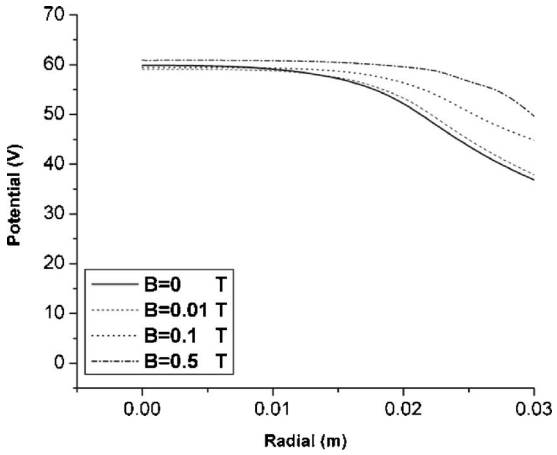

FIG. 16. Time-averaged potential profiles in the bulk in the plane of symmetry, for different values of the magnetic field. There is no enhanced radial component of the electric field in the quasineutral bulk; the gradient in the potential is practically the same for different values of the magnetic field.

axis. The thick black lines indicate the gradient in the force at these balance points. Note that for the magnetic-field-free discharge, the force balance occurs far away from the discharge center, as was indicated by the local dust density maximum in Fig. 8. For the discharges with large magnetic fields, the force balance lies much closer to the discharge center.

We see that the change in the ion density profiles has an important effect on the transport of dust in the discharge. The

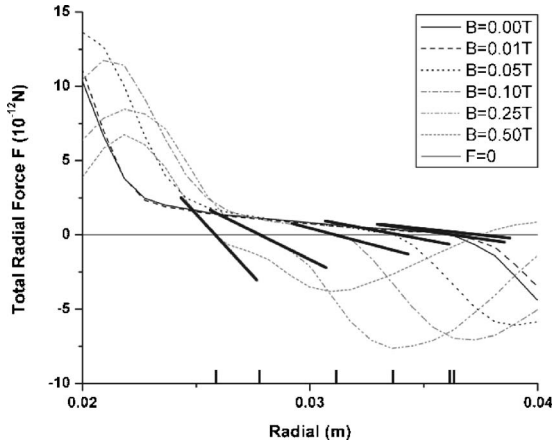

FIG. 15. The net force acting on dust particles in the radial direction in the plane of symmetry at $Z=0.027$ m. The point where the forces balance is indicated by the black lines on the horizontal axis. The large black lines indicate the gradient in the force at the points where the total force vanishes. For small magnetic fields, the gradient in the force does not change much, as is shown in Fig. 14. However, the force balance points move inwards, due to the different ion density profile. For high magnetic fields, the force close to the force balance points becomes larger. The total effect is faster dust transport towards the force balance points and a smaller distance between the initial dust particle positions (below and above the electrodes) and the force balance points, which leads to shorter void-formation times.

magnetic field does not change the mobility and diffusion of the ions directly, however, since the ions are too heavy to be magnetized by the magnetic fields used in the simulations. In order to understand the change in the ion density profiles, we analyze the differences in ion transport in the next section.

Since we calculate the drift velocity of the dust assuming that the friction with the neutrals balances all other forces, there cannot be an overshoot followed by a damped oscillation when the dust moves toward the equilibrium point. In case the friction is too low, the frequency of the oscillations is also affected by the magnetic field. The stronger derivative of the net force will increase the oscillation frequency with increasing magnetic field. We are not able to study this within the context of our model. This is also true for dust vortices, often observed in dusty plasmas under microgravity. However, the force field calculated to simulate the dust transport does show vortices when used to track single dust particles, as was shown in [33]. The results were similar to the theoretical calculations performed in [34]. We also do not consider Brownian motion of dust particles around equilibrium positions, which might affect the true transport time scales involved. However, for the distances over which the dust is transported in our simulation, the effect of Brownian motion will not be a dominant transport mechanism.

VI. ION TRANSPORT AND "AMBIPOLAR" DIFFUSION

One possibilty for the large radially extended bulk in the ion density is an increase in the effective electric field in the bulk. Figure 16 shows the electric potential. We see the growth of the quasineutral, equipotential bulk of the discharge. There does not seem to be a large change in the gradients of the potential. We conclude at first sight that there is no change in the time-averaged radial electric field in the bulk, large enough to explain the change in the ion density profile.

Another explanation would be a change in ionization. Figure 13 shows that the total number of ions does not change

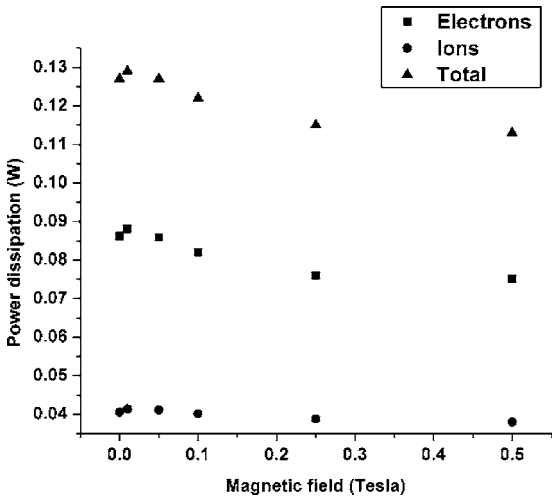

FIG. 17. The dissipated power for the electrons, ions, and the total dissipated power for different values of the magnetic field, indicating the level of ionization. The dissipated power hardly changes, which means that the total ionization in the discharge remains the same for increasing magnetic field.

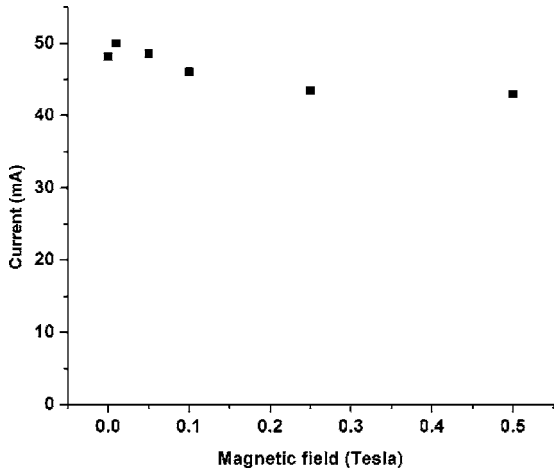

FIG. 18. The current to the electrodes for different values of the magnetic field. The current to the electrodes does not change, which means that the current towards the outer walls does not change as well (the total current has to be conserved). Thus, the current distribution in the discharge does not show an important change for increasing magnetic field.

very much. A change in ionization will also be reflected in a change in the dissipated power in the plasma. Figure 17 shows the dissipated power.

We see that the dissipated power remains about the same for different values of the magnetic field, ±0.1 W. There is no change in the total ionization in the discharge large enough to explain the difference in the ion density distribution.

Another explanation could be a change in the currents; maybe more current is directed to the outer wall, instead of to the electrodes, leading to more Ohmic heating of electrons in the radial direction, causing more ionization radially than axially. However, the current to the electrodes, plotted in Fig. 18, also remains equal. There is no important change in the current distribution inside the discharge with an applied magnetic field, which can explain the change in the ion density distribution.

The only remaining explanation is therefore a change in the diffusion of positive ions in the bulk toward the outer wall. The diffusion in the quasineutral bulk will be mainly *ambipolar diffusion*. Ambipolar diffusion is based on the equality of the electron and ion fluxes, together with the assumption of quasineutrality. In a dusty plasma this reads $n_+e=n_ee+eZ_Dn_D$ and the equations for the ambipolar diffusion have to be changed accordingly [35,36]. However, when the dust particles are introduced, the ion drag forcing them to move "around the void" is mainly due to ions diffusing out of the bulk of the discharge, where no dust is present. The ions will therefore diffuse out of the bulk with a diffusion coefficient equal to the normal ambipolar diffusion coefficient,

$$D_a = \frac{\mu_i D_e + \mu_e D_i}{\mu_e + \mu_i}. \tag{25}$$

Using Eq. (17), we notice that the ambipolar diffusion coefficient is reduced when the electrons become magnetized. Fig. 19 shows a plot of the electron-magnetized ambipolar diffusion coefficient for the discharge parameters used in the simulation. Without magnetic field, the ambipolar diffusion coefficient reduces to the classical value for $\mu_e \gg \mu_i$; $D_a=D_i(1+T_e/T_i)$, which is indicated by the dashed line. For very large magnetic fields, the ambipolar diffusion coefficient approaches the magnetized electron diffusion coefficient, indicated by the dot-dashed line.

We can also rewrite the equality of fluxes in the bulk to derive the *ambipolar electric field*. The result for electropositive discharges [37] is

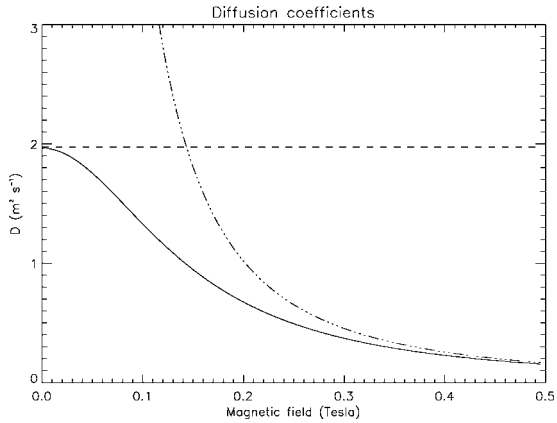

FIG. 19. Radial ambipolar diffusion coefficient for different magnetic-field strengths. Solid line is the ambipolar diffusion, dashed line the magnetic-field-free value, and the dot-dashed line the magnetized electron diffusion coefficient. We see that for higher magnetic fields, the diffusion of ions out of the bulk becomes less, because of the magnetization of the electrons, and approaches the *magnetized electron* diffusion.

TABLE I. The calculated ambipolar electric field according to Eq. (26) and the effective electric field found from the model according to Eqs. (3) and (4) for different values of the applied axial magnetic field, **B**. We see that in the bulk of the discharge, the effective electric field is given by the ambipolar electric field. The flux of plasma particles in the bulk of the discharge is therefore the ambipolar flux. The magnetic field reduces the ambipolar electric field in the bulk and thus the ambipolar flux of plasma particles out of the bulk of the discharge.

B (T)	Ambipolar field (V/m)	Bulk field (V/m)
0	239	240
0.01	140	150
0.05	100	125
0.1	52	60
0.25	38	42
0.5	19	20

$$\mathbf{E}_{\mathrm{amb}} = -\frac{d\ln(n_{+,e})}{dx}\left(\frac{D_e - D_+}{\mu_e + \mu_+}\right). \tag{26}$$

Comparing the calculated ambipolar electric field with the time-averaged electric field in the bulk found from the simulations, we find a good agreement, as shown in Table I.

Since the total ionization remains the same, while the diffusion of the ions is reduced for higher magnetic field, the area between the electrodes fills up with ions, resulting in the cigar-shaped bulk. The total current to the outer wall is the same, however, as Fig. 18 shows. This means that the gradient in the ion density must increase, since the flux of ions in the bulk is now given by the ambipolar diffusive flux,

$$\mathbf{\Gamma}_i = -D_a\frac{\partial n_i}{\partial x}. \tag{27}$$

We indeed see that the ion density gradient near the edge of the void increases with increasing magnetic field and thus with decreasing ambipolar diffusion. We need to consider one more thing, namely a possible change in the charging of the dust particles in the presence of a magnetic field, for instance by a change in the electron orbits.

A. Effect of magnetic field on charging

As was mentioned in the abstract, the effect of the magnetic field on the charge of dust particles can be neglected. This is important for the interaction between dust particles, and thus for the formation of voids as well. In [38] it was mentioned that a magnetic field can have an important effect on the charge of dust particles. The charge is first reduced when the electrons are magnetized and the electron cyclotron radius becomes smaller than the capture radius of the dust particles as derived by OML theory; $r_d > r_c$. For an electron orbiting with a constant cyclotron radius, there are two degrees of freedom, namely the translational direction, parallel to the magnetic field, and the azimuthal direction, perpendicular to the magnetic field. Assuming that the total thermal energy is evenly distributed over the kinetic energy, i.e.,

$$k_B T_e = \frac{1}{2}m_e v_e^2 = \frac{1}{2}m_e(v_\perp^2 + v_\parallel^2) = \frac{1}{2}m_e(2v_\perp^2), \tag{28}$$

we rewrite this, by using $v_\perp = \omega_{c,e} r_c$, as

$$r_c B = \frac{m_e}{e}\sqrt{\frac{k_B T_e}{m_e}}, \tag{29}$$

which means that for a change in the charging of dust particles by the magnetization, we can find the critical magnetic field as

$$r_d B > \frac{m_e}{e}\sqrt{\frac{k_B T_e}{m_e}}. \tag{30}$$

Filling in the numbers, this gives

$$r_d\ (\mu\mathrm{m}) B\ (\mathrm{T}) > 2.386\sqrt{T_e\ (\mathrm{eV})}, \tag{31}$$

which was also stated by Tsytovich *et al.* in their article, but in units of kG [38]. The critical magnetic field for the ions is $\mu = \sqrt{m_i T_i / m_e T_e}$ times higher. In our simulations, the dust particle radius is 6.8 μm. The typical electron energy is a few eV. This means that the critical magnetic-field strength is approximately 0.6 T. In our simulations, we stayed below this value and therefore we conclude that the magnetic field does not have an important effect on the charging of the dust particles. Therefore, we can still use the OML theory to calculate the dust charge [Eqs. (7) and (8)].

VII. COMPARISON WITH THE PLANET FORMATION REGION

We start by considering the magnetization of the ions and electrons in the dusty plasma around the YSO. Using the literature [39], we find the values for the neutral density, temperature, and the magnetic field: $n_n \approx 10^{15}\ \mathrm{m}^{-3}, T_n \approx 100\ \mathrm{K}, B \approx 10^{-3}\ \mathrm{T}$, so that we can calculate the electron momentum transfer frequency and electron cyclotron frequency as $\nu_{m,e} \approx 10^6$ Hz and $\omega_{c,e} \approx 10^8$ Hz. So, $\beta_e \gg 1$ as in our simulations. For the ion species we assume that hydrogen will be the most common element. Taking a density of $10^{17}\ \mathrm{m}^{-3}$ [39] and estimating that hydrogen is $\sqrt{m_{\mathrm{Ar}^+}/m_{\mathrm{H}^+}} \approx 6$ times more mobile than the argon used in our model [40], we find a momentum transfer frequency of $\nu_{m,\mathrm{H}} \approx 10^7$ Hz, whereas the cyclotron frequency is $\omega_{c,\mathrm{H}} \approx 10^5$ Hz, so $\beta_{\mathrm{H}} \ll 1$ as in our simulations.

The dust particle diameters as observed in [9,10] and as observed in meteorites on Earth as the so called "chondrites" are all in the μm range [41]. Therefore, our choice of a radius of 6.8 μm fits well within the range of these observations.

The source of ionization in a star formation region around a YSO consists of ionization by cosmic rays and by the intense UV flux originating from the YSO. The remaining energy of the UV photon after the ionization will almost completely be picked up by the electron, leaving a cold population of ions and a hot population of electrons. This will lead to charge separation and ambipolar diffusion. Even though the experiment in our model has walls at which the plasma ends, the local ionization and transport of plasma

particles in the quasineutral part is similar. In the space environment, plasma will recombine once the average energy of the electrons has become low enough. The surrounding neutral background can then be considered "the walls" around the plasma. The role of ionization by UV radiation in a dusty plasma has been discussed in [42].

In our model, we use a fluid description of the plasma and dust particles. This can be done since in the size of the experiment (L) many collisions of the plasma particles under consideration occur. The so called Knudsen number l/L is very small, with l the mean free path of the particles, which is in the order of a millimeter. In the planet formation region, l is much larger, due to the low background density. However, the size of the dusty plasma is hundreds of a.u.'s. There are many collisions of plasma particles with the background. The only difference would involve the time scales on which collisions occur.

The process of planet formation includes the process of the actual formation of micrometer-sized dust particles through the coagulation of weakly charged, nanometer-sized particulates, which involves weak, short- range forces. However, a large part of the planet formation process involves the coagulation of larger, micrometer-sized dust particles. These particles will carry a significant charge and therefore the plasma-particle and interparticle forces will dominate over weak, short-range forces and the transport of dust particles through the plasma becomes important. We have shown that a magnetic field plays an important role in the transport of plasma and dust particles in low-temperature plasmas, which shares many parameters with the dusty plasmas around YSO's. The better confinement of electrons as compared to ions creates regions where the ratio of the ion and electron density becomes so high that the dust may even get a positive charge, thus enhancing coagulation. We therefore conclude that magnetic fields will play an important role in the transport of dust particles, thus in the possibility of coagulation of these dust particles and in the process of planet formation in general.

VIII. CONCLUSIONS

We have used a fully self-consistent 2D model to solve the transport of plasma particles and dust particles in a low-temperature rf argon discharge under microgravity conditions in the presence of a homogeneous magnetic field in the axial direction. This model includes ionization, excitation, and recombination on dust particles, together with an approach to account for the change in dust diffusion when a crystalline region is formed.

We have discussed the importance of the ion drag force. After a careful analysis of recent theoretical and experimental results, we argue that the approach of Barnes *et al.* to compute the ion drag force, taking the electron Debye length as the cutoff length, is still qualitatively appropriate to describe the ion drag force.

We have shown that a magnetic field in a low-pressure rf discharge under microgravity conditions has important consequences for the transport of plasma particles and consequently for the transport of dust. The electrons are magnetized and their perpendicular mobility and diffusion coefficient is reduced. This also reduces the ambipolar diffusion of plasma particles out of the quasineutral bulk of the discharge. Already at low magnetic fields the ion density profiles are affected and the quasineutral large bulk covers a larger part of the area between the electrodes. For high magnetic fields, a large gradient in the ion density builds up. This moves the point where all the forces acting on the dust particles cancel inward, away from the wall. The large gradient in the ion density results in a large gradient in the total force around this point where the forces balance. The combined effect of the reduced distance that injected dust particles have to travel before reaching force balance, and the increased force they experience close to this point results in a reduction of the time scale on which a closed void is formed, for increasing magnetic field. The direct effect of the magnetic field on the charging of dust particles can be neglected; changes are only due to the different plasma background.

Even though in the rf reactor the loss of ions to the wall is the reason for the ion transport, we showed that there are many collisions in the plasma before the ions reach the wall. We also showed that the main transport mechanism in the bulk of the plasma is ambipolar diffusion. In YSO's this ambipolar diffusion is most likely the main source for plasma transport. Since so many features of the modeled experiment coincide with those of a YSO dusty plasma and since the discussed mechanism depends so strongly on the ambipolar diffusion in the bulk and not on the properties of the plasma at the walls, we believe that the presence of a magnetic field around YSO's has an important effect on dust transport time scales and therefore on time scales involving planet and star formation. We believe that it is worthwile to check these findings in future low-temperature rf experiments, extended with an applied magnetic field.

ACKNOWLEDGMENTS

This work, supported by the European Communities under the contract of Association between EURATOM/FOM, was carried out within the framework of the European Fusion Programme with financial support from NWO. The views and opinions expressed herein do not necessarily reflect those of the European Commission.

[1] J. P. Goedbloed and S. Poedts, *Principles of Magnetohydrodynamics with Applications to Laboratory and Astrophysical Plasmas* (Cambridge University Press, Cambridge , 2004).
[2] G. S. Selwyn, J. Singh, and R. S. Benett, J. Vac. Sci. Technol. A **7**, 2758 (1989).
[3] M. Meaudre, R. Meaudre, R. Butté, and S. Vignoli, J. Appl. Phys. **86**, 946 (1999).
[4] P. Roca i Cabarrocas, J. Non-Cryst. Solids **266–269**, 31 (2000).
[5] U. Kortshagen and U. Bhandarkar, Phys. Rev. E **60**, 887 (1999).
[6] K. de Bleecker, A. Bogaerts, and W. Goedheer, Phys. Rev. E **70**, 056407 (2004).
[7] M. Z. Jacobson and J. H. Seinfeld, Atmos. Environ. **38**, 1839 (2004).
[8] W. E. Amatucci, D. N. Walker, G. Gatling, and E. E. Scime, Phys. Plasmas **11**, 5, (2004).
[9] Y. K. Okamoto *et al.*, Nature (London) **431**, 660 (2004).
[10] C. M. Telesco *et al.*, Nature (London) **433**, 133 (2005).
[11] G. E. Morfill *et al.*, Phys. Rev. Lett. **83**, 1598 (1999).
[12] A. P. Nefedov *et al.*, New J. Phys. **5**, 33.1 (2003).
[13] M. R. Akdim and W. J. Goedheer, Phys. Rev. E **67**, 066407 (2003).
[14] I. Revel *et al.*, J. Appl. Phys. **88**, 2234 (2000).
[15] J. E. Allen, Phys. Scr. **45**, 497 (1992).
[16] G. Gozadinos, A. V. Ivlev, and J. P. Boeuf, New J. Phys. **5**, 32.1 (2003).
[17] M. Zuzic *et al.*, Phys. Rev. Lett. **85**, 4064 (2000).
[18] M. Mitcher, *Partially Ionized Gases* (John Wiley & Sons, New York, 1973).
[19] S. A. Khrapak *et al.*, Phys. Rev. E **66**, 046414 (2002).
[20] M. S. Barnes *et al.*, Phys. Rev. Lett. **68**, 313–316 (1992).
[21] M. D. Kilgore *et al.*, J. Appl. Phys. **73**, 7195 (1993).
[22] C. Zafiu, A. Melzer, and A. Piel, Phys. Plasmas **10**, 5 (2003).
[23] S. A. Khrapak *et al.*, Phys. Plasmas **10**, 11 (2003).
[24] C. Zafiu, A. Melzer, and A. Piel, Phys. Plasmas **10**, 11 (2003).
[25] M. Klindworth, A. Piel, A. Melzer, U. Konopka, H. Rothermel, K. Tarantik, and G. E. Morfill, Phys. Rev. Lett. **93**, 195002 (2004).
[26] A. V. Ivlev *et al.*, Phys. Rev. Lett. **92**, 205007 (2004).
[27] A. V. Ivlev *et al.*, Phys. Rev. E **71**, 016405 (2005).
[28] M. R. Akdim and W. J. Goedheer, Phys. Rev. E **65**, 015401(R) (2002).
[29] M. Lampe *et al.*, Phys. Rev. Lett. **86**, 5278 (2001).
[30] M. Lampe *et al.*, Phys. Plasmas **10**, 1500 (2002).
[31] V. N. Tsytovich and G. E. Morfill, Plasma Phys. Controlled Fusion **46**, B527 (2004).
[32] S. Ichimaru, Rev. Mod. Phys. **54**, 1017 (1982).
[33] M. R. Akdim and W. J. Goedheer, Phys. Rev. E **67**, 056405 (2003).
[34] O. S. Vaulina, A. A. Samarian, O. F. Petrov, B. W. James, and V. E. Fortov, New J. Phys. **5**, 82 (2003).
[35] J. X. Ma *et al.*, Phys. Plasmas **9**, 5 (2002).
[36] Sh. Amiranashvili and M. Y. Yu, Phys. Plasmas **9**, 11 (2002).
[37] R. N. Franklin, J. Phys. D **36**, 828 (2003).
[38] V. N. Tsytovich, N. Sato, and G. E. Morfill, New J. Phys. **5**, 43.1 (2003).
[39] G. T. Birk., Astron. Astrophys. **330**, 1070 (1998).
[40] E. W. McDaniel, *Collision Phenomena in Ionized Gases* (John Wiley & Sons, New York, 1964).
[41] M. Zolensky *et al.*, Meteorit. Planet. Sci. **38**, 305 (2003).
[42] V. E. Fortov *et al.*, New J. Phys. **5**, 102.1 (2003).